FINAL REPORT

Spatial Mapping of Ozone Production in San Antonio

AQRP Project 17-032

Prepared for:
Gary McGaughey
Texas Air Quality Research Program
The University of Texas at Austin

Prepared by:
Ezra Wood (Principal Investigator)
Department of Chemistry
Drexel University

September 2017

QA Requirements: Audits of Data Quality: 10% Required

ACKNOWLEDGMENT
The preparation of this report is based on work supported by the State of Texas through the Air Quality Research Program administered by The University of Texas at Austin by means of a Grant from the Texas Commission on Environmental Quality.

Executive Summary

Ozone formation rates and mechanisms have not been previously studied in San Antonio. Due to peak observed O_3 values that are close to the National Ambient Air Quality Standard, gaining an understanding of ozone formation rates and chemical mechanisms is important for eventually designing effective ozone abatement programs. Measurements of total peroxy radicals ($[HO_2] + [RO_2]$, "[ROx]") were made during May 2017 in three sites upwind and downwind of San Antonio: at the University of Texas-San Antonio, which is in the Northwest of San Antonio, Floresville (Southeast of San Antonio), and Corpus Christi (Southeast of San Antonio). Combined with measurements of NO, ozone production rates were calculated for the three-week measurement project. Peroxy radicals were measured by the Ethane CHemical AMPlifier method (ECHAMP), housed in the Aerodyne Mobile Laboratory. Additionally, a thermal dissociation cavity attenuated phase shift spectrometer (TD-CAPS) was installed in the AML to measure organic nitrates. These measurements were combined with those made by collaborators at Aerodyne Research, Inc., including the radical precursors ozone, water vapor, formaldehyde, and acetaldehyde, as well as photolysis rate constants (actinic flux) to investigate the nature of ozone formation in the greater San Antonio area.

Major findings of these measurements and preliminary analysis include the following:

1. Daytime ozone production rates were typically between 5 and 10 ppb/hr and rarely exceeded 15 ppb/hr. The highest $P(O_3)$ values were observed in air masses with elevated P(HOx) and [NO] values ([NO]>0.3 ppb).

2. Primary radical production rates P(HOx) were dominated by the reaction of $O(^1D)$ with water vapor (following the photolysis of ozone) and the photolysis of formaldehyde with much smaller contributions measured or inferred from the photolysis of acetaldehyde, hydrogen peroxide, acetone, and nitrous acid. HOx radical production from alkene ozonolysis and atomic chlorine formation from photolysis of nitryl chloride ($ClNO_2$) and molecular chlorine (Cl_2) have not been quantified. Peak P(HOx) values observed were 0.6 – 0.7 ppt/s – less than half that previously observed in Houston in photochemically active air masses.

3. Analysis of estimated contributors to the HOx destruction rate L(HOx) suggests that $P(O_3)$ was almost always NOx-limited during the 3-weeks of measurements. Similarly, the dependence of $P(O_3)$ on [NO] and P(HOx) suggests that $P(O_3)$ was usually NOx-limited, and this occurs when [NO] is less than 600 ppt at the highest P(HOx) values observed (greater than 0.5 ppt/s) or less than 200 ppt at lower P(HOx) values (less than 0.25 ppt/s). During the few time periods when $P(O_3)$ was likely NOx-saturated, absolute $P(O_3)$ values were usually low – less than 5 ppb/hr.

4. During the few days that alkyl nitrates and peroxy nitrates were measured by TD-CAPS, alkyl nitrates accounted for a much smaller portion of total nitrogen oxides (NO_Y) than peroxy nitrates.

These conclusions are based on three weeks of measurements in San Antonio when there was usually southeasterly flow. Although high O_3 events are more often observed during

southeasterly flow compared to other flow patterns, we cannot yet quantitatively address how representative these measurements were of other time periods.

Recommendations for Future Analysis

Based on the preliminary analysis of the field data collected for this project, there are two main topics that warrant further analysis that would greatly inform our understanding of current and future ozone pollution in San Antonio:

1. The dependence of ozone formation on NOx, VOCs, and HOx production rate should be analyzed using data collected at the upwind (Floresville, Corpus Christi), downwind (UTSA), and urban (Traveler's World) sites during the San Antonio Field Study. This will involve greatly expanding the preliminary analysis in this report. For example, the role of "non-traditional" radical sources such as alkene ozonolysis and the photolysis of nitryl chloride ($ClNO_2$) and molecular chlorine (Cl_2) has not been investigated. Similarly, the absolute $P(O_3)$ values and their dependence on NOx in the urban core have not been investigated.

2. The impact of future trends of NOx and VOC emissions on ozone concentrations and formation rates upwind of and inside San Antonio should be analyzed. This will involve analyzing emissions data, trends, and future projections for multiple emission sources (on-road, electricity generation, oil & gas activities, cement kilns, etc.), including satellite data, in concert with photochemical models.

Table of Contents

Table of Figures

1. Introduction

San Antonio's ozone values are near the national ambient air quality standard (NAAQS) of 70 ppbv (8-hour average). As a result, regulators will need to make science-based decisions on effective mitigation strategies, including emission reduction programs. Such decisions will require knowledge of the amount of ozone that is transported into the city from upwind (usually Southeast of San Antonio), the absolute rates of ozone formation in and around San Antonio, the relative importance and interaction of various emission sources (e.g., upwind oil and gas activity and urban emissions from the city itself), and when and where ozone formation is NOx-limited or VOC-limited. In contrast to Houston and Dallas, little is known about ozone formation in San Antonio.

Ozone is formed by photochemical reactions involving volatile organic compound (VOCs) and nitrogen oxides (NOx). The photo-oxidation of propane (a component of natural gas) serves as a simple example of this chemistry:

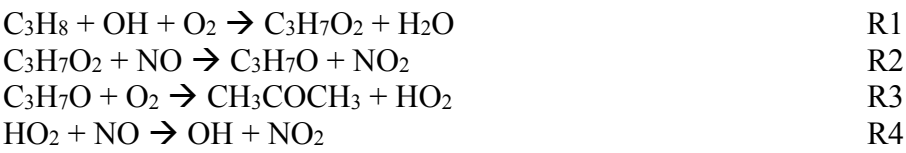

$C_3H_8 + OH + O_2 \rightarrow C_3H_7O_2 + H_2O$ R1
$C_3H_7O_2 + NO \rightarrow C_3H_7O + NO_2$ R2
$C_3H_7O + O_2 \rightarrow CH_3COCH_3 + HO_2$ R3
$HO_2 + NO \rightarrow OH + NO_2$ R4

The NO_2 formed by reactions 2 and 4 will undergo photolysis during the day, thereby forming ozone (O_3):

$NO_2 + \text{sunlight} \rightarrow NO + O$ R5
$O + O_2 + M \rightarrow O_3 + M$ R6

Thus the rate at which ozone is formed is effectively equal to the rate at which NO is converted to NO_2 by reaction with peroxy radicals (in this case, $C_3H_7O_2$ and HO_2):

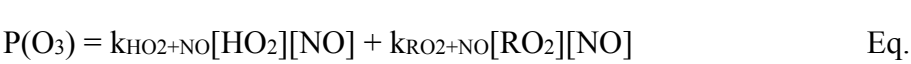

$P(O_3) = k_{HO2+NO}[HO_2][NO] + k_{RO2+NO}[RO_2][NO]$ Eq. 1

"RO_2" represents all organic peroxy radicals (e.g., CH_3O_2, $C_2H_5O_2$, etc.)

Due to the various radical termination steps such as formation of H_2O_2 and HNO_3, the value of $P(O_3)$ does not always simply increase with increased concentrations of VOCs or NOx. Ozone production is said to be "NOx-limited" if, due to low NO concentrations, peroxy radicals react with themselves rather than with NO. Conversely, ozone formation is "VOC-limited" (or "NOx-saturated") if HOx radicals (OH, RO_2, HO_2) are mainly lost via reactions with NO_X. Knowing in which chemical regime an air mass resides is crucial for designing effective ozone abatement strategies, since reducing NOx emissions can lead to undesirable *increases* in ozone formation rates if the air is in a VOC-limited state. This is the case in southern California, evident by the higher ozone observed on weekends when there is reduced NOx emissions due to lower diesel truck traffic [1].

The science goals for this project are listed below:

1. What are the rates of instantaneous ozone production ($P(O_3)$) upwind, within the urban core, and downwind of San Antonio? During what times of day and where (upwind/downwind) is $P(O_3)$ NOx-limited vs. VOC-limited?

2. What is role of alkanes in O_3 formation? Alkanes comprise the majority of VOC emissions from oil and gas activities but not urban or biogenic emissions.

2. Project Design

To address the above science questions, Drexel Researchers integrated two analytical instruments into the Aerodyne Mobile Laboratory (AML) – one that measures total peroxy radicals (RO_2 and HO_2) and another that measures organic nitrates. The AML made measurements at three different locations in the greater San Antonio area between May 11 and May 31, 2017 as shown in Figure 1.

1. University of Texas at San Antonio, 14 miles northwest of downtown San Antonio.
2. Floresville, 30 miles southeast of San Antonio
3. Lake Corpus Christi State Park, 100 miles southeast of San Antonio and 40 miles inland from the Gulf of Mexico

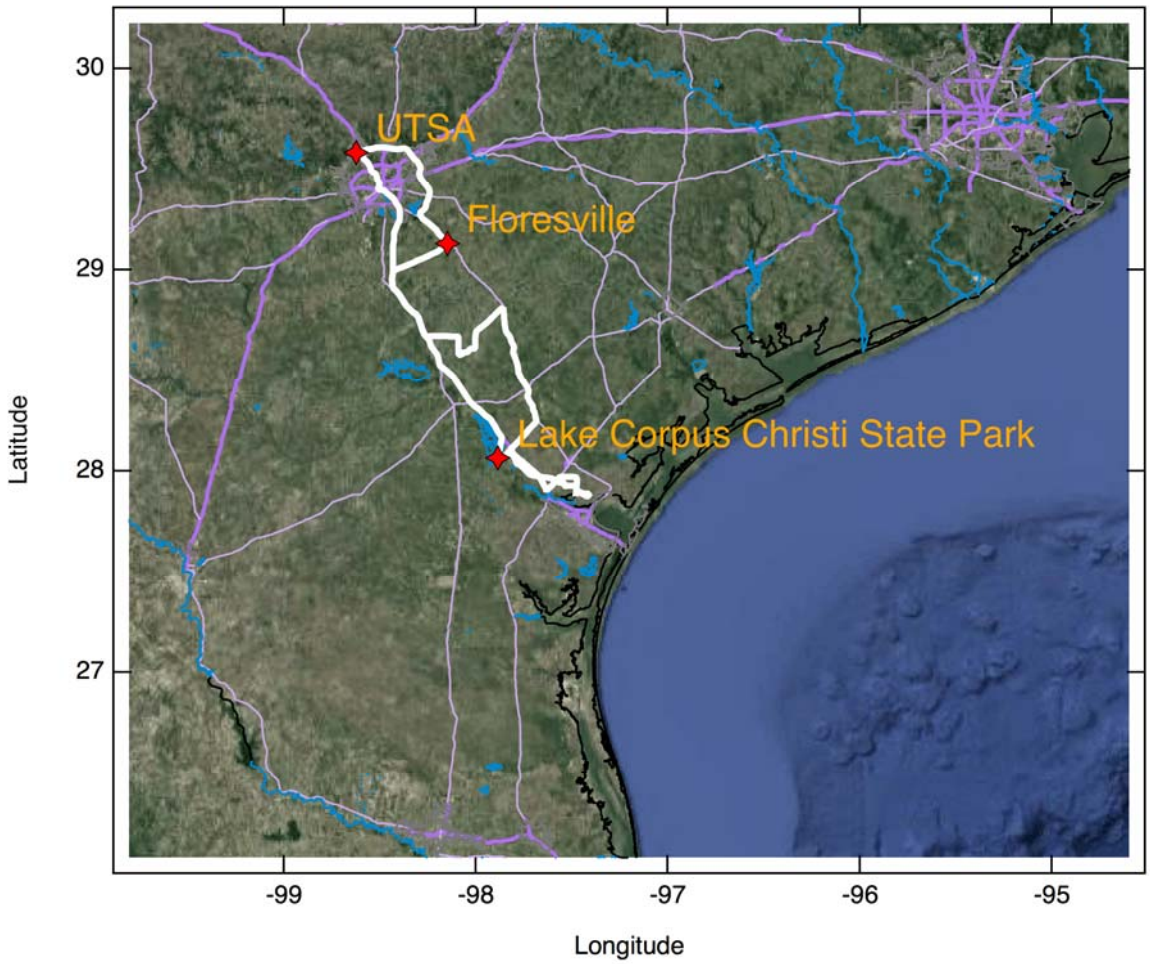

Figure 1. Measurement Locations for Project 17-032.
The red diamond symbols indicate the locations where the mobile labs were stationed.

Under the most common southeasterly wind patterns, Corpus Christi and Floresville are upwind of San Antonio and UTSA is downwind. The instantaneous rate of ozone production $P(O_3)$ in ppb/hr was calculated using the measurements of peroxy radicals and nitric oxide and equation 1.

3. Experimental Methods

ECHAMP measurements of total peroxy radicals

The sum of the hydroperoxy radical (HO_2) and organic peroxy radicals (RO_2, where R is an organic fragment, e.g. CH_3O_2, $C_2H_5O_2$), henceforth referred to as "ROx", was measured by the Ethane CHemical AMPlifier (ECHAMP) technique [2]. This technique is based on the conversion of the reactive peroxy radicals into a higher concentration of less reactive nitrogen dioxide (NO_2), which is then measured by cavity attenuated phase shift spectroscopy (CAPS) [3]. To effect this conversion, sampled air is mixed with high concentrations of ethane (C_2H_6) and nitric oxide (NO), leading to the following reactions:

$HO_2 + NO \rightarrow OH + \mathbf{NO_2}$ R7
$OH + C_2H_6 + O_2 \rightarrow C_2H_5O_2 + H_2O$ R8
$C_2H_5O_2 + NO \rightarrow C_2H_5O + \mathbf{NO_2}$ R9
$C_2H_5O + O_2 \rightarrow CH_3CHO + HO_2$ R10

The HO_2 produced by reaction 10 can then react with NO again (reaction 7). For each completion of the chain represented by the four reactions above, two NO_2 molecules are produced. Due to radical termination steps (not shown) the effective amplification factor is 15 at a relative humidity of 50%, meaning that for each HO_2 sampled, 15 NO_2 molecules are produced. This NO_2 amplification product is then detected by cavity attenuated phase shift spectroscopy (CAPS) – a highly sensitive NO_2 detection method [3]. Two reaction chambers are required – at any given point in time, one is in "amplification mode" while the other is in a background mode. The ROx concentration is determined by the difference between these two CAPS NO_2 readings and the amplification factor F:

$[ROx] = [NO_2](amplification) – [NO_2](background) / F$

This technique is similar to the "traditional" chemical amplification technique ("PERCA" [4]) which used carbon monoxide rather than ethane. The use of ethane reduces the dependence of the calibration factor on relative humidity and also greatly facilitates deployment due to the marked reduction in reagent toxicity. The C_2H_6 cylinder concentration was 40% (balance nitrogen), which dilutes to 1.4% in the FEP reaction chambers. The NO cylinder concentration was 40 ppm (balance nitrogen), which dilutes to 1 ppm in the FEP reaction chambers.

A schematic of the inlet box is shown in figure 2.

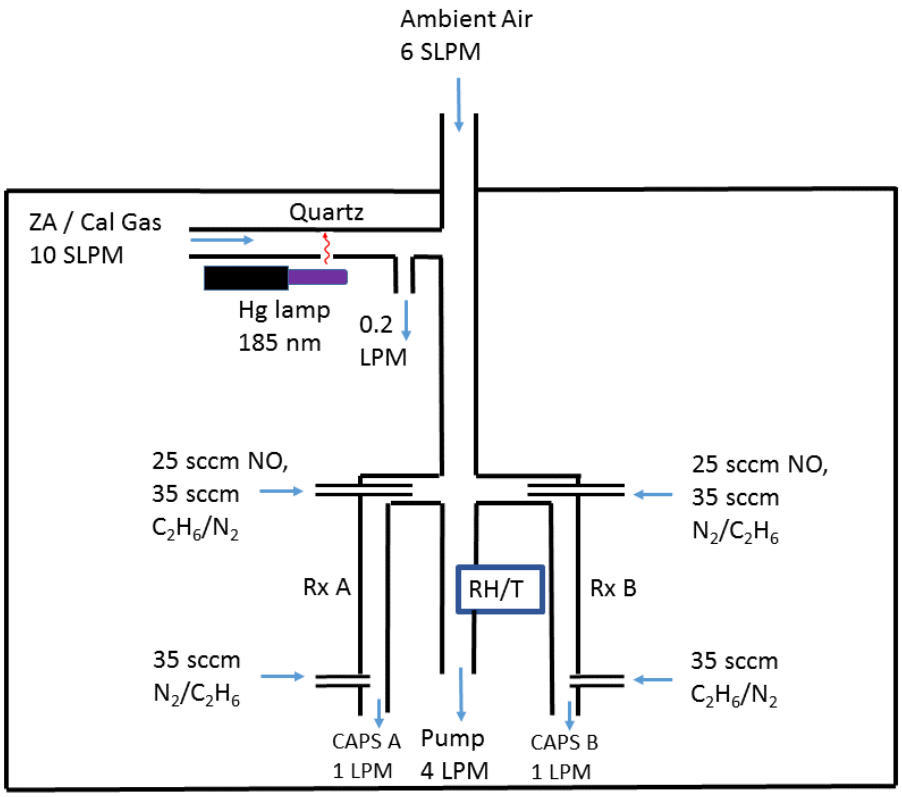

Figure 2. Schematic of the ECHAMP Inlet Box.
Amplification chemistry occurs in the inlet box. A calibration source based on H_2O photolysis is integrated into the inlet box and can be operated remotely. The NO_2 amplification product then flows through 75 feet of FEP tubing into the CAPS sensors which are housed inside the Aerodyne Mobile Laboratory.

For the San Antonio deployment, the inlet box was attached to the same sampling structure onto which all AML sampling inlets were attached, at a height of 10 meters (figure 3).

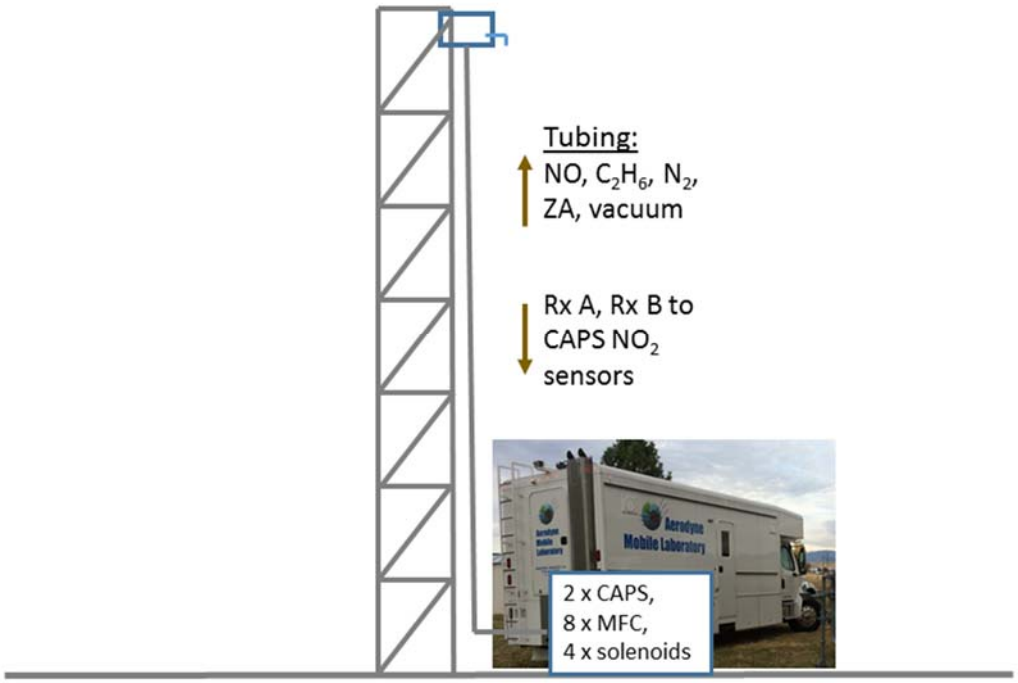

Figure 3. Sampling Schematic.
The ECHAMP inlet box was positioned at a height of 10 m, affixed to a sampling structure. Peroxy radicals were converted into NO_2 with an "amplification" factor of 10 – 15 and then transported through tubing to dual CAPS NO_2 sensors in the Aerodyne Mobile Laboratory.

The amplification factor F of the instrument is determined using two different calibration methods - one based on the photolysis of water vapor and one based on the photolysis of methyl iodide (CH_3I). The water photolysis method was performed on six dates, whereas the CH_3I method was performed once on the last day of the project. The results of these calibrations are presented in the quality assurance section. Briefly, the two methods agreed to within 15%, and indicate an amplification factor of 22 under dry conditions that decreased to 15 at a relative humidity (RH) of 42%. Additionally, the CAPS NO_2 sensors require calibration. This was performed before, during, and after the project by quantitative conversion of O_3 produced by an O_3 calibration source (2B model 306).

The uncertainty of the ROx measurements is described in Wood et al., and determined mainly by the NO_2 calibration uncertainty, the need to interpolate and extrapolate amplification factor (F) values at RH values for which calibrations were not performed, and the kinetic and spectroscopic parameters needed for the two calibration methods. The 2σ uncertainty of the measurements is 27%. The precision (and detection limit) of the measurements depends largely on the relative humidity (because of the dependence of the amplification factor on RH) and the precision of the CAPS NO_2 measurements. The 1σ precision was typically 2-3 ppt for 2 minute average measurements during the day (RH typically 30 to 75%) and up to 6 ppt at night (when the RH often exceeded 75%). The resulting signal-to-noise values were typically 10 or higher for daytime measurements ([ROx]>30 ppt) but rarely over 3 at night.

TD-CAPS measurements of organic nitrates

Organic nitrates were measured by Thermal-Dissociation Cavity Attenuated Phase Shift spectrometry (TD-CAPS). This technique is based on sampling air into a heated quartz inlet, causing organic nitrates to decompose into an organic fragment and NO_2, which is then detected by a CAPS NO_2 sensor. The types of organic nitrates that thermally decompose depends on the temperature set point for the quartz tube. Acyl peroxy nitrates of the general form RO_2NO_2, the most common of which is peroxy acetyl nitrate ("PAN", $CH_3C(O)OONO_2$), decompose at approximately 200° C:

RO_2NO_2 + heat → RO_2 + NO_2

Whereas alkyl nitrates and hydroxy alkyl nitrates of the general form $RONO_2$ decompose at approximately 300 °C:

$RONO_2$ + heat → RO + NO_2

This technique has been described in detail by researchers who have used other methods to detect the NO_2 thermal dissociation product, including laser-induced fluorescence [5, 6]and cavity attenuated phase shift spectroscopy [7].
Figure 4 shows a thermal recorded while sampling air from the Colorado State U. "smog chamber" during experiments on wood smoke oxidation during October 2016. A schematic of the sampling system is shown in figure 5.

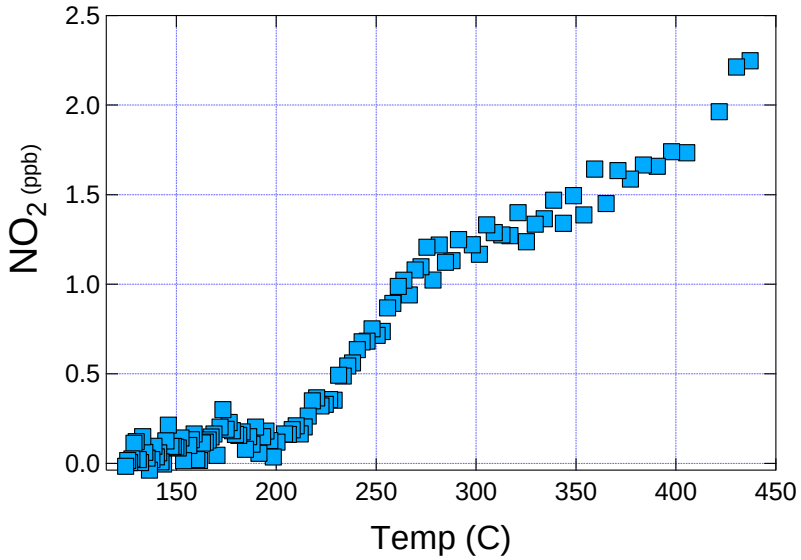

Figure 4. Thermogram of TD-CAPS inlet.
In this particular application, an activated carbon gas-phase denuder was used to remove gas-phase NO_2 and organic nitrates while passing particulate organic nitrates. A denuder was not used for the AQRP measurements.

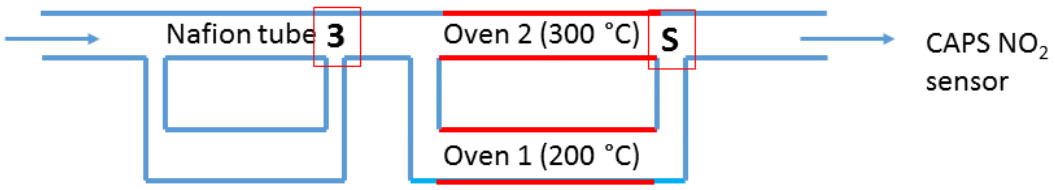

Figure 5. Schematic of the TD-CAPS sampling lay-out.
"3" = Three-way valve. "S" = three-way solenoid valve.

Calculated quantities: P(HOx), $P(O_3)$.

The gross ozone production rate $P(O_3)$ was calculated by the following equation:
$P(O_3) = 8.5 \times 10^{-12} ([RO_2]+[HO_2])][NO]$

The coefficient of 8.5×10^{-12} is an average value for the rate constant for HO_2 + NO and RO_2 + NO for small organic RO_2 [8], in cm^3 $molecule^{-1}$ s^{-1}, with an estimated 2σ uncertainty of 15%.

The 2σ uncertainty on this $P(O_3)$ calculated value, using the quadrature sum of the uncertainties for the three factors (15%, 27%, and 5%), is 31%.

The HOx radical production rate (where "HOx" is defined as OH + HO_2 + RO_2) from the photolysis of O_3, HCHO, CH_3CHO, and H_2O_2 is calculated by the following equation:

$$P(HOx) = 2j_{(O1D)}[O_3](k_{O1D+H2O}[H_2O]/(k_{O1D+H2O}[H_2O] + k_{O1D+O2}[O_2] + k_{O1D+N2}[N_2]) + 2j_{HCHO \rightarrow H + CHO}[HCHO] + 2j_{CH3CHO \rightarrow CH3 + HCO}[CH_3CHO] + 2j_{H2O2}[H_2O_2]$$

The contribution of acetone photolysis was not included but spot inspections indicate a minor role (< 3% of total P(HOx)). Alkene ozonolysis and HONO photolysis have not been included but should be for a more refined analysis.

4. Results

A time series of showing mixing ratios of O_3, NO, ROx, $j_{O3 \rightarrow O(1D)}$, and calculated $P(O_3)$ on May 12 and 13 at the UTSA site is shown in figure 6.

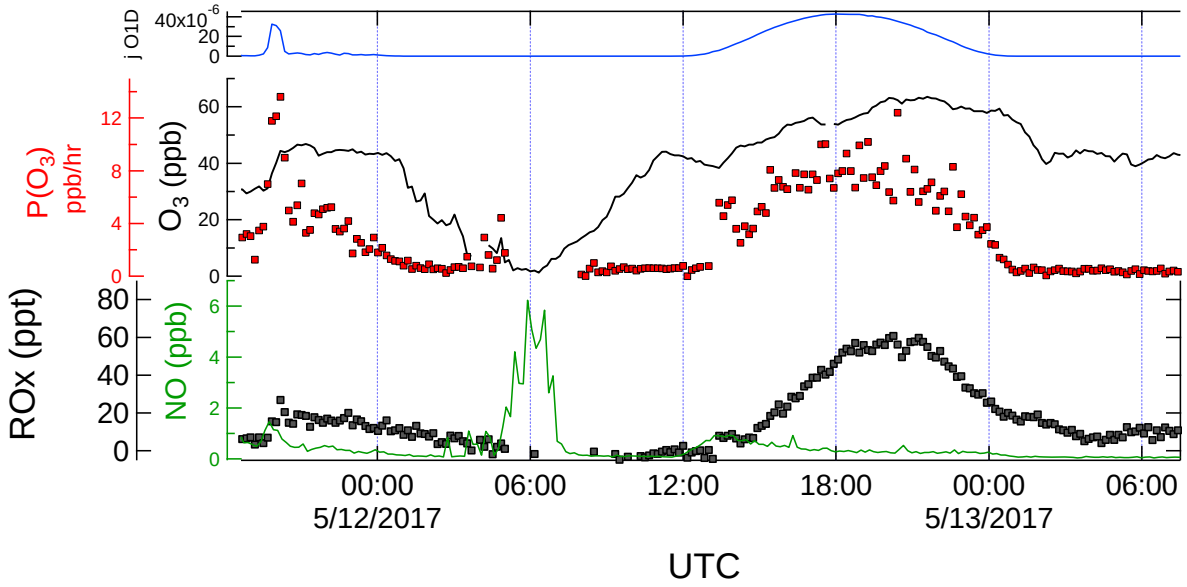

Figure 6. Time series of [NO], [ROx], [O_3], j_{O1D}, and $P(O_3)$ on May 12 and 13that UTSA. Time shown is Universal Time (= Local time + 5 hours). All measurements are 10-minute averages.

5/12 was a mostly overcast day with only a brief period of sun as indicated by the top trace ($j_{O3 \rightarrow O(1D)}$ photolysis rate). During the overcast periods, the resulting ROx mixing ratios and $P(O_3)$ values were less than half that observed on the following, sunny day. The brief period of sun on 5/12 coincided with relatively high NO mixing ratios ([NO]> 1 ppb), leading to the highest $P(O_3)$ values observed on either day (12 – 14 ppb/hr).

Similar data from all five days during the first UTSA measurements are shown below. The highest $P(O_3)$ values of 15 – 20 ppb/hr were observed on 5/15/2017, when daytime [NO] was between 0.3 to 0.5 ppb, compared to approximately 0.2 the preceding three days.

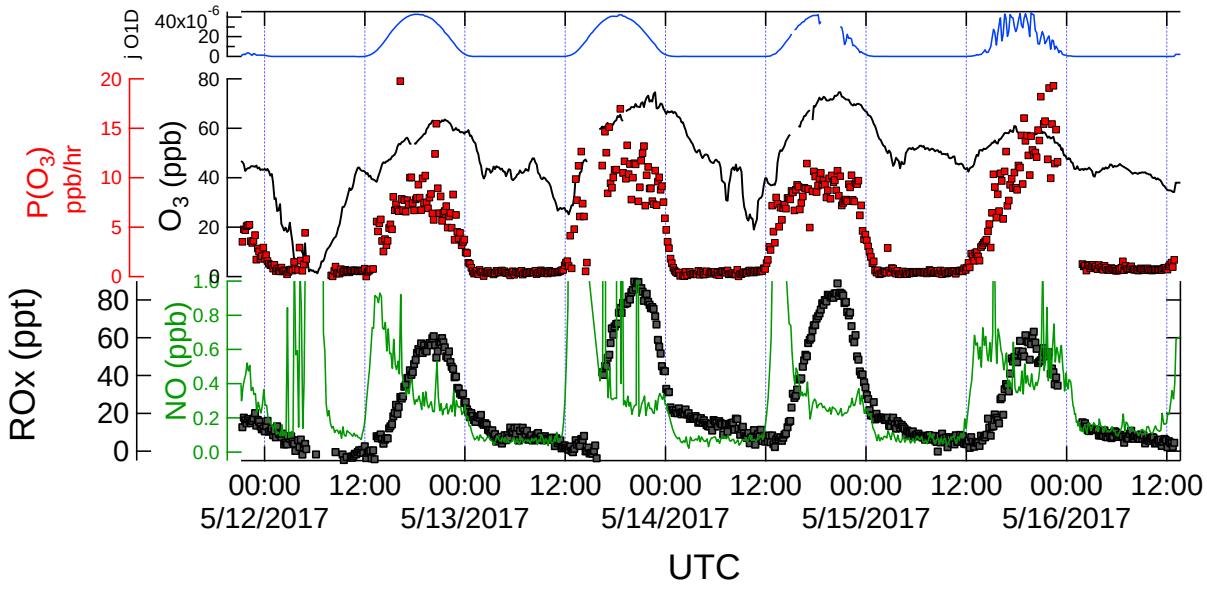

Figure 7. Time series of [NO], [ROx], [O_3], j_{O1D}, and $P(O_3)$ at UTSA.

$P(O_3)$ values were lower at the Floresville and Corpus Christi sites as shown in figures 8 and 9:

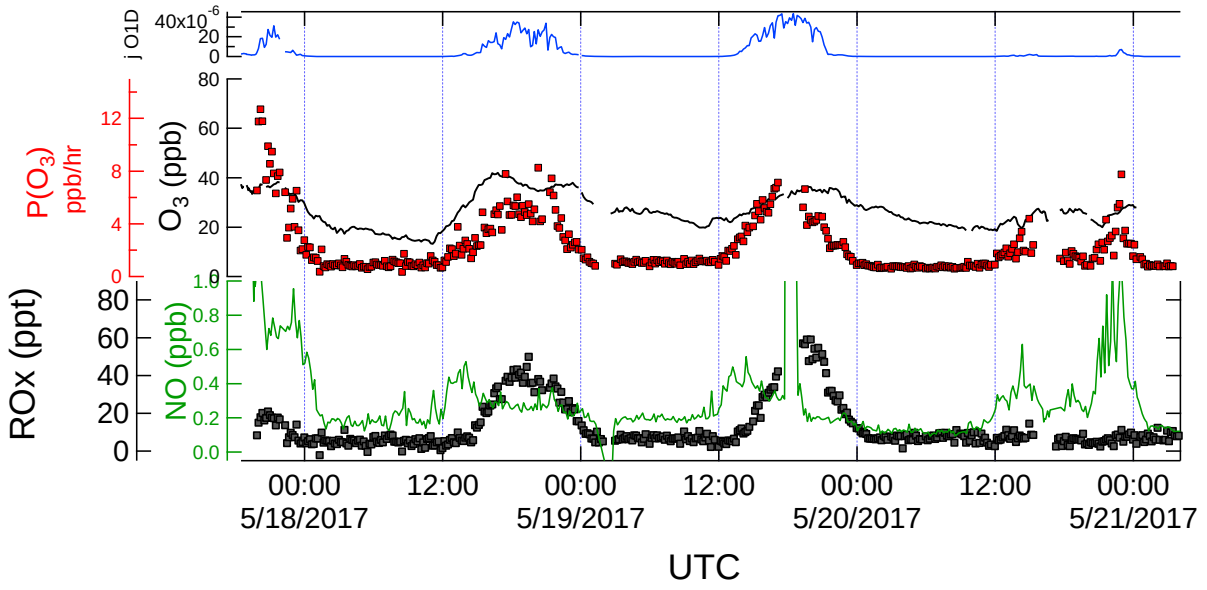

Figure 8. Measurements at the Floresville site.

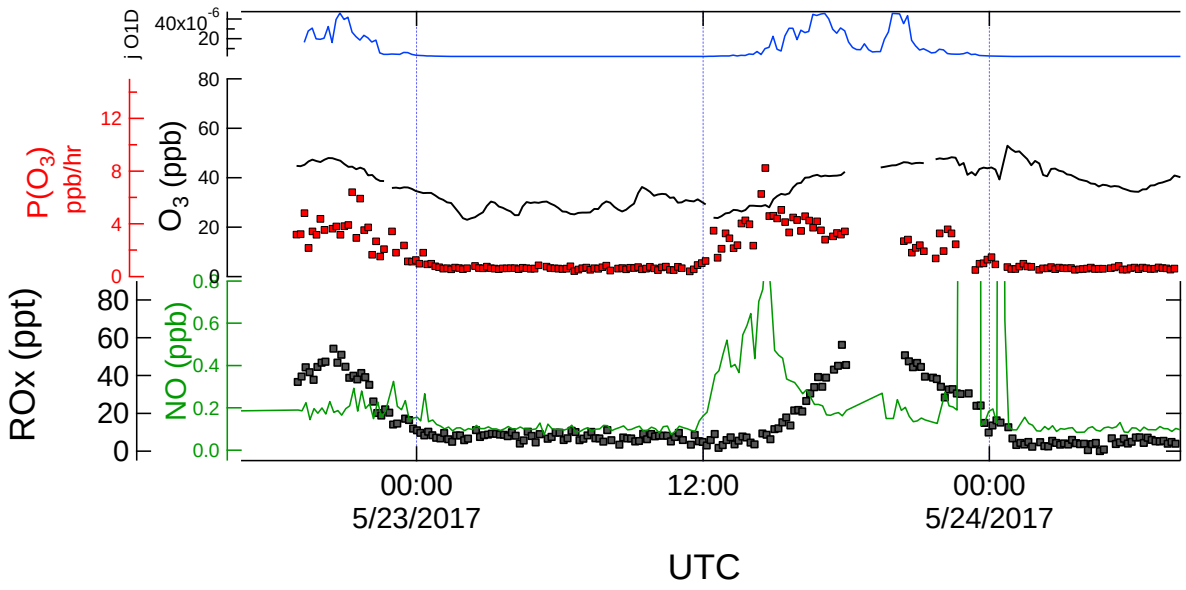

Figure 9. Measurements at the Corpus Christi site.

P(HOx) and P(O_3) for the entire project are displayed in Figure 10:

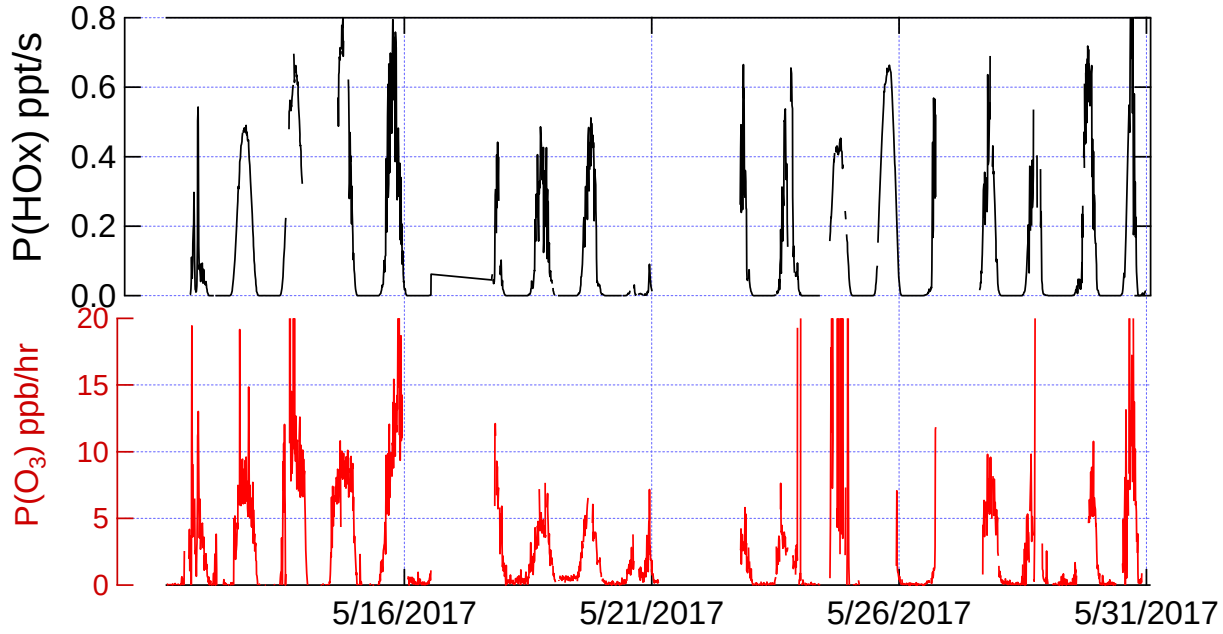

Figure 10. P(O_3) and P(HOx) for the entire project.
P(HOx) was calculated using measured photolysis rates and the radical precursors O_3, H_2O, HCHO, CH_3CHO, and H_2O_2.

The TD-CAPS system suffered a few experimental setbacks and as a result data are only available for the last few days of the project. Measurements of total acyl peroxy nitrates

("ΣPNs") were successful and showed adequate signal-to-noise, however the alkyl nitrate ($RONO_2$) measurements showed much lower concentrations and will require more refined analysis. Overall it is apparent, however, that alkyl nitrates were a much smaller component of NOy than peroxy nitrates.

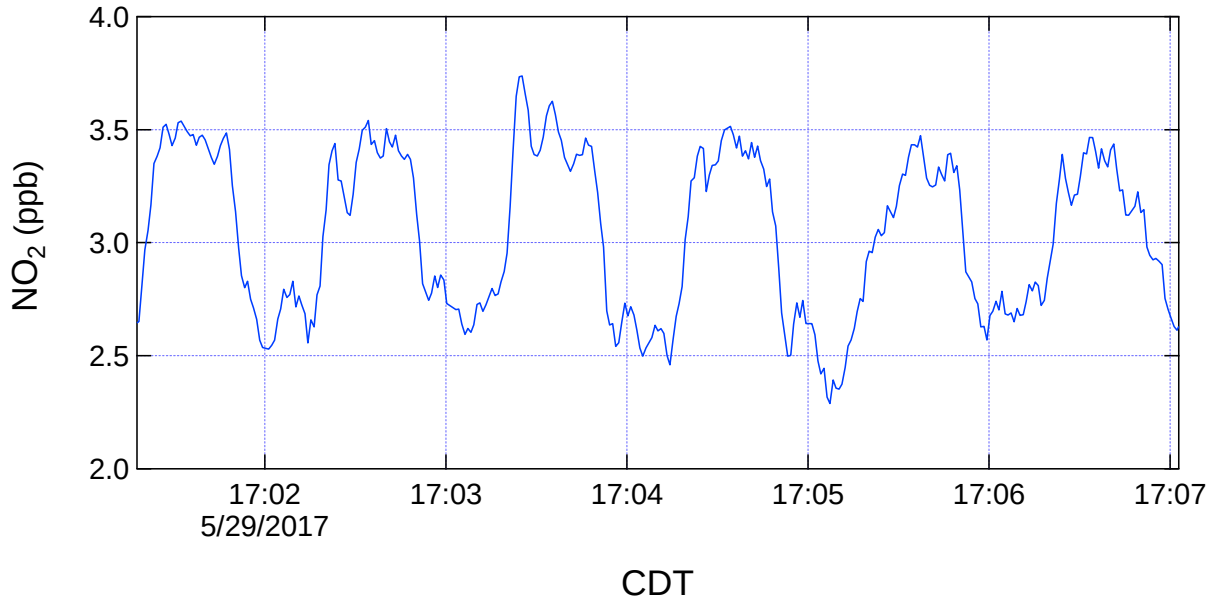

Figure 11. TD-CAPS measurements of total peroxy nitrates.
[ΣPNs] (PAN, PPN, MPAN, etc.) *is equal to the difference in [NO_2] between sampling through the 200 °C quartz tube and unheated quartz tube, and equal to 0.8 ppb in the time window shown.*

An additional measurement that was attempted was measurement of alkyl peroxy radicals – i.e., only organic peroxy radicals formed from alkane oxidation and without the contribution of hydroxy- peroxy radicals that are formed by the oxidation of alkenes and aromatic compounds. This was attempted by sampling through a nafion membrane tube, and required the entire sampling tower to be brought down. Laboratory experiments have indicated efficient removal by the nafion tube of HO_2 and the β-hydroxy peroxy radicals formed from isoprene oxidation, but near unit transmission of methyl and ethyl peroxy radicals. One of the field tests of this sampling method was compromised by emissions from local lawnmower emissions. A second test showed an increase in the ROx signal. The interpretation of these results will require further laboratory investigation.

5. Preliminary Analysis

The $P(O_3)$ values calculated from the measured NO and ROx in the greater San Antonio area were "moderate", with values rarely exceeding 20 ppb/hr. In contrast, $P(O_3)$ values determined either by measurements or models have routinely exceeded 50 ppb/hr in the Houston-Galveston area [9, 10]. For example, during the 2006 TRAMP study in Houston, the median mid-day $P(O_3)$ value solely from the reaction of HO_2 with NO was 40 ppb/hr [9]. The total $P(O_3)$ value can be estimated as twice that, assuming RO_2 and HO_2 concentrations were comparable. Median, mid-day P(HOx) values during TRAMP were 1.2 ppt/s, roughly twice that observed at the San Antonio sites. There are many reasons for these difference, including higher O_3, NOx, HONO, and HCHO mixing ratios in Houston.

Of importance for designing effective emission reduction control programs is knowledge of whether ozone formation occurs under NOx-limited or NOx-saturated conditions. Two types of analysis are used to assess which chemical regime ozone formation occurs in the greater San Antonio area: Analysis of radical budgets and analysis of the dependence of $P(O_3)$ on P(HOx) and NO.

Analysis of radical budgets

Under NOx-limited conditions, ROx radicals are destroyed mainly by self-reactions:

$HO_2 + HO_2 \rightarrow H_2O_2 + O_2$
$HO_2 + RO_2 \rightarrow ROOH + O_2$

Whereas under NOx-saturated conditions, ROx radicals are removed by reactions between ROx radicals and NOx:

$OH + NO_2 + M \rightarrow HNO_3 + M$
$RO_2 + NO + M \rightarrow RONO_2 + M$

By quantifying the rates of these reactions, the NOx-limited vs. NOx-saturated nature of ozone production can be determined. Many of the important compounds in the above reactions, however, were not individually measured. The sum of HO_2 and RO_2 were measured rather than each one separately, and OH was not measured. To estimate these rates, we assume that the measured peroxy radicals were 50% HO_2 and 50% RO_2, and that the effective chain terminating rate constant for $RO_2 + HO_2$ to form hydroperoxides ROOH (versus other reactions that simply convert HO_2 and RO_2 into other forms of ROx radicals) is equal to 6×10^{-12} cm^3 $molecule^{-1}$ s^{-1}. For comparison, the rate constants for the reaction $HO_2 + CH_3O_2 \rightarrow CH_3OOH + O_2$, $HO_2 + HOCH_2O_2$, and $HO_2 + C_2H_5O_2$ are 5.2×10^{-12}, 1.2×10^{-11}, and 7.8×10^{-11} cm^3 $molecule^{-1}$ s^{-1}, respectively. An [OH] concentration of 3×10^6 molecules cm^{-3} was used for estimating the rate of $OH + NO_2$, and an overall $RONO_2$ yield for the reaction of RO_2 with NO of 6% was assumed.

These calculated values and their sum are compared to the total P(HOx) value calculated using the photolysis rate constants and radical precursors (O_3, H_2O, HCHO, CH_3CHO, H_2O_2) in figures 12 and 13.

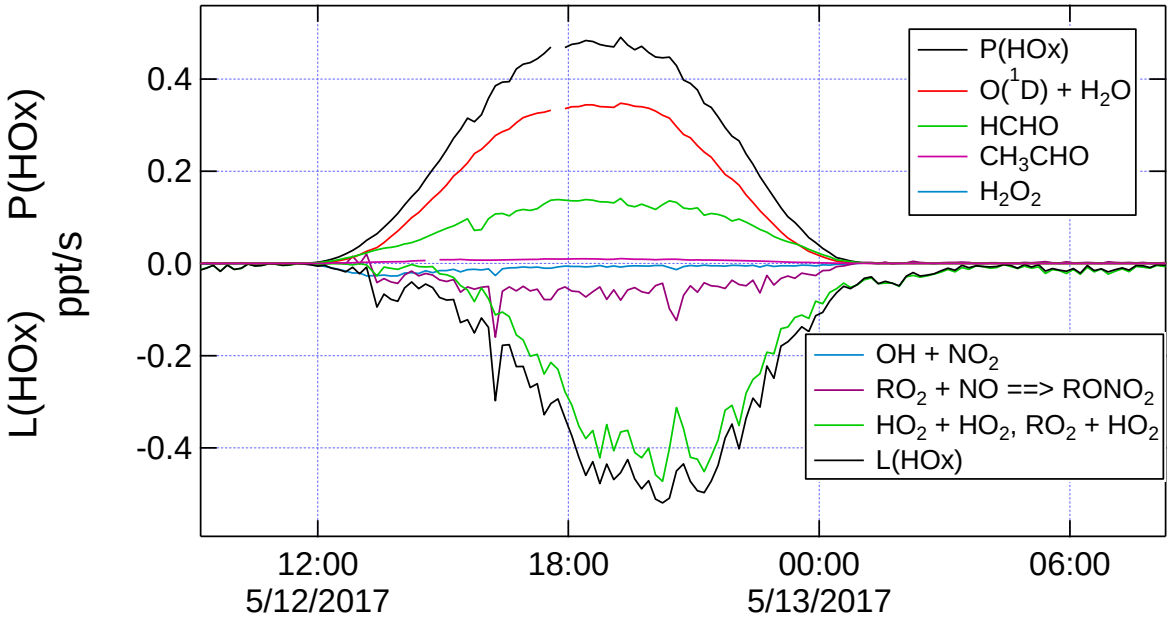

Figure 12. Calculated/Estimate P(HOx) and L(HOx) values on 5/12/2017.
Overall P(HOx) and L(HOx) are comparable, and HOx-NOx reactions account for a small portion of total L(HOx), suggesting that P(O_3) was strongly NOx-limited that day.

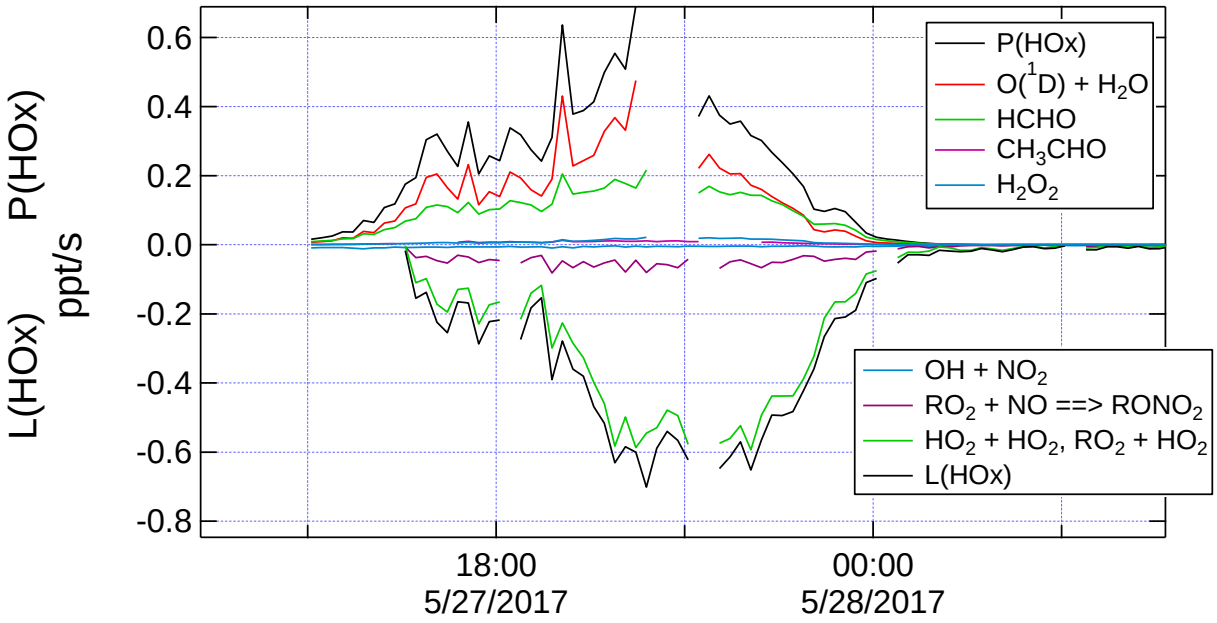

Figure 13. P(HOx) and L(HOx) for 5/27/2017.

For both days shown, there is rough agreement between P(HOx) and L(HOx), although P(HOx)>L(HOx) in the morning. This morning disagreement likely is due to "missing" HOx loss processes or from an overestimate of the j_{HCHO} and $j_{O3 \rightarrow O(1D)}$ rate constants. Nevertheless, it

is apparent that the HOx-NOx reactions, i.e., formation of HNO_3 and $RONO_2$, account for much less than 50% of total L(HOx). Even if OH were actually 10 times higher at an unrealistic value of 3×10^7 molecules cm^{-3}, HNO_3 formation would still be smaller than L(HOx) estimated from $HO_2 + HO_2$ and $HO_2 + RO_2$. For the HOx-NOx reactions to account for over 50% of L(HOx), all the estimates used for these calculations would need to be greatly in error.

Dependence of $P(O_3)$ on NO and P(HOx).

As discussed in the introduction, at fixed P(HOx) and [VOC] values, $P(O_3)$ is expected to increase with NO at low NO values and, after reaching a "transition" [NO] value, decrease with continued increases in [NO]. Under NOx-limited conditions, the VOC reactivity is not expected to affect $P(O_3)$, but increases in P(HOx) are always expected to increase $P(O_3)$. The dependence of $P(O_3)$ on NO and P(HOx) is shown in figure 14.

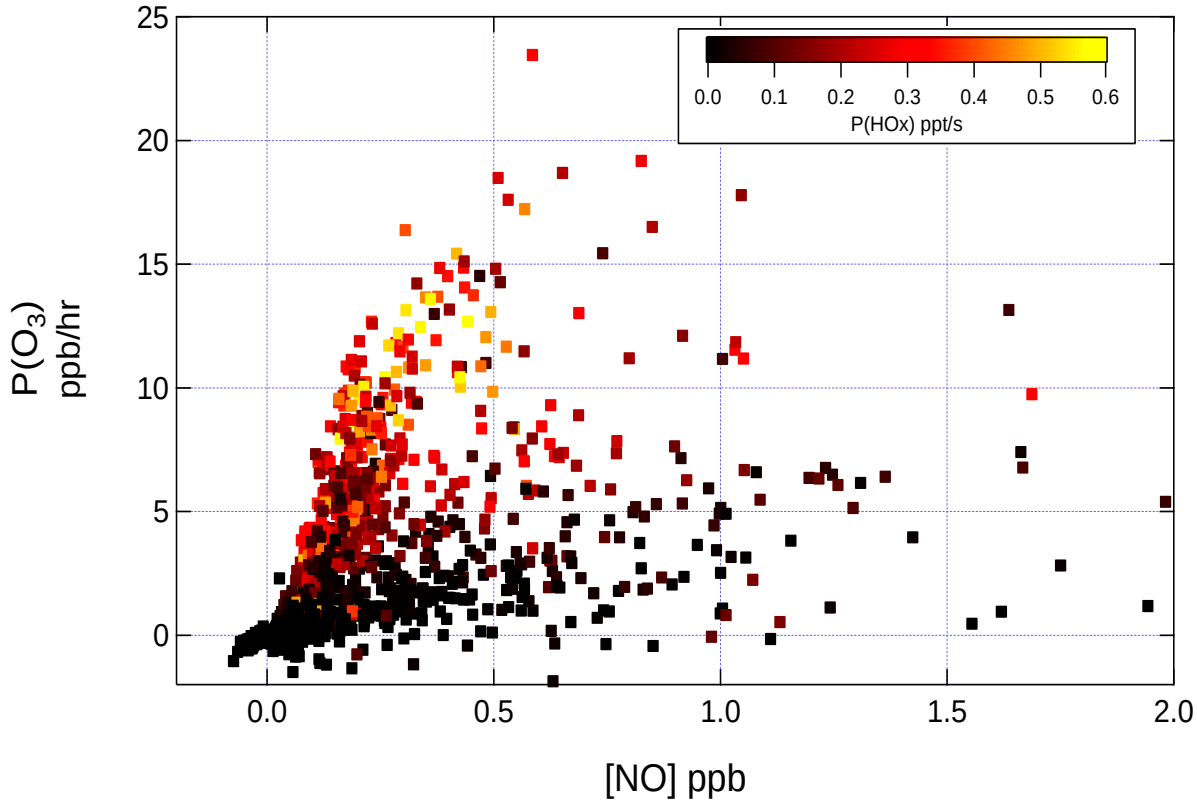

Figure 14. Dependence of $P(O_3)$ on NO, colored by P(HOx), for all the data collected during the San Antonio project.

Evident from figure 14 is that $P(O_3)$ increases w/ NO at low [NO] (roughly at [NO]< 0.5 ppb). To further investigate this dependence, for figure 15 the median $P(O_3)$ measurements in bins corresponding to 50 ppt increments in NO are shown, and split into three P(HOx) categories: low P(HOx) (less than 0.25 ppt/s), medium P(HOx) (between 0.25 and 0.5 ppt/s), and high P(HOx) (greater than 0.5 ppt/s).

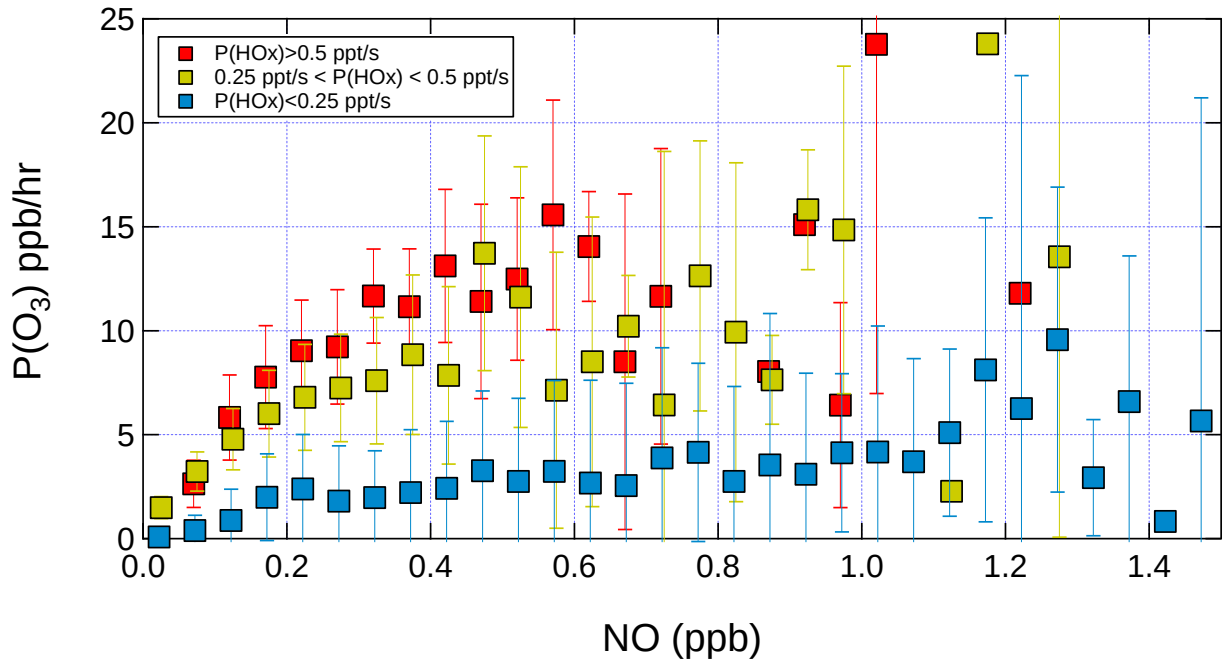

Figure 15. Dependence of $P(O_3)$ on NO and P(HOx).
Each point is the median value within 50 ppt NO increments.

Figure 15 demonstrates that at low P(HOx), $P(O_3)$ increases w/ [NO] up until about 200 ppt, at which $P(O_3)$ appears to be mostly uncorrelated w/ NO. Similarly, for medium and high P(HOx) values, transition NO mixing ratios of approximately 400 and 600 ppt are observed.
The "noise" in the data above 600 ppt NO is a result of both the small number of measurements for which daytime NO exceeded 600 ppt, and the fact in the NOx-saturated portion of the graph the VOC concentrations are expected to affect $P(O_3)$.

Figure 15 suggests that $P(O_3)$ was NOx-saturated for NO values that exceeded these transition values. A histogram of measured NO values is shown in figure 16, and shows that only a small portion of measurements had NO exceeding 0.5 ppb. Even when $P(O_3)$ was NOx-saturated at the low P(HOx) values, which only requires that NO > 200 ppt, the absolute values are very low – less than 5 ppb/hr.

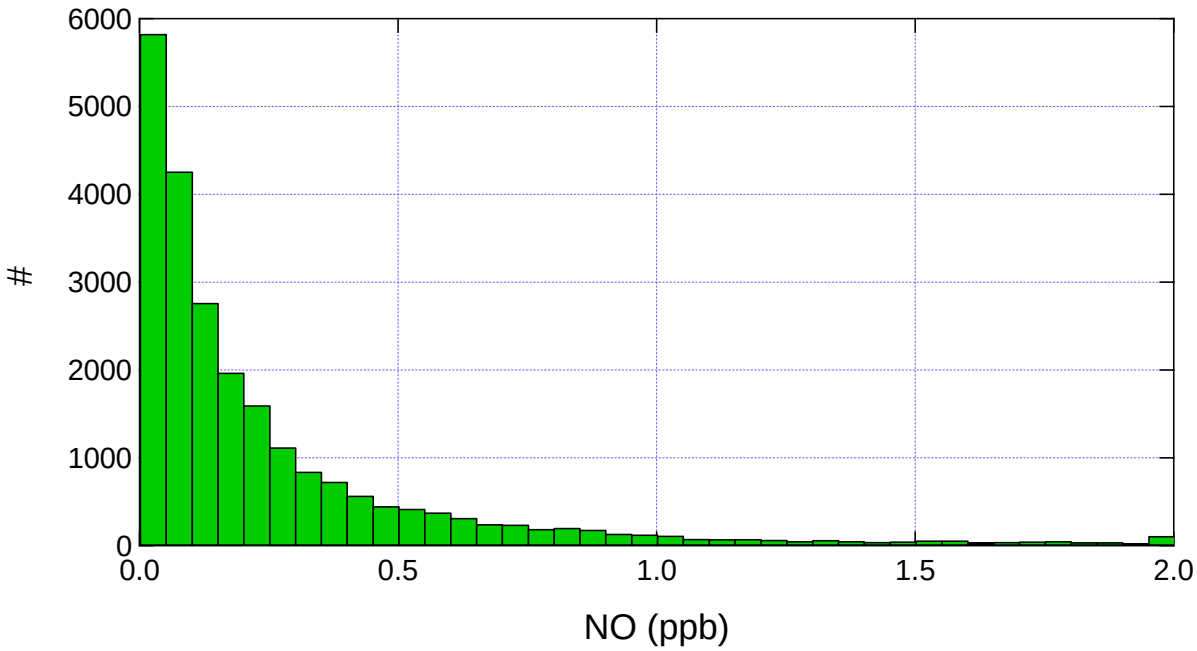

Figure 16. Histogram of 10-minute NO mixing ratios from all measurement sites.

As demonstrated above, $P(O_3)$ was mostly NOx-limited at all three measurement sites. NOx concentrations recorded by the network of NOx monitors are higher at sites in the urban core of San Antonio, however. Sites 678 and 27 are both inside the 410 loop, and show NOx concentrations that are higher than those measured at the other sites by up to a factor of 10 depending on time of day. As a result, it is possible that during days with southeasterly flow, $P(O_3)$ is NOx-limited in air upwind of the city, increases in magnitude as NOx from urban sources is emitted into the air and possibly becomes NOx-saturated, and decreases by the time the air arrives at the upwind site both due to dilution of NOx and photochemical processing. Increases in $P(O_3)$ will likely occur in upwind areas if NOx increases in those areas, e.g. the Eagle Ford Shale. An increase of ~30% in the satellite-observed NO_2 column has been observed between 2005 and 2014 over the Eagle Ford Shale play [11].

6. Audits of Data Quality

a. One of the most difficult aspects of any measurement of ROx radicals is the need to calibrate the instrument – that is, to produce a known concentration of radicals that is sampled by the instrument. We use two methods that are intrinsically very different and whose uncertainties are based on completely different physical quantities.

The water vapor photolysis is based on the photolysis of water vapor at 185 nm [12]:

H_2O + 184.9 nm → H + OH
H + O_2 + M → HO_2 + M

In the presence of H_2 (5 sccm of 100% H_2 diluted into 10 LPM of zero air, resulting in a diluted mixing ratio of 500 ppm), the OH is rapidly converted to HO_2:

OH + H_2 + O_2 → H_2O + HO_2

The resulting peroxy radical concentration is given by equation 5:

$$[HO_2] + [RO_2] = 2[H_2O]\sigma_{H2O}\Phi_{H2O}Ft \qquad \text{Eq. 5}$$

Where σ_{H2O} is the water vapor absorption cross section at 184.9 nm, Φ_{H2O} is the photolysis quantum yield at 184.9 nm (equal to one), F is the lamp photon flux, and t is the gas exposure time. Most commonly, research groups determine Ft either directly (i.e., using a calibrated photodiode), or rely on N_2O or O_3 chemical actinometry [13]. Ozone chemical actinometry takes advantage of the fact that ozone is also produced by photolysis of O_2 by the same wavelength as OH and HO_2 are produced by photolysis of H_2O. Thus knowledge of the relevant spectroscopic parameters for O_2 and quantification of [O_3] can be used to determine Ft:

$$[HO_2] + [RO_2] = \frac{[O_3][H_2O]\sigma_{H2O}\varphi_{H2O}}{[O_2]\sigma_{O2}\varphi_{H2O}} \qquad \text{Eq. 6}$$

where the σ and Φ values are the absorption cross sections and photolysis quantum yields for H_2O and O_2 at 184.9 nm. The effective absorption cross section of O_2 depends on the oxygen column depth and lamp operating parameters and has been quantified for our Hg lamp [14], with a value of 1.3×10^{-20} cm^2 $molecule^{-1}$.

The CH_3I photolysis method is similar to that described by Liu et al. [15]

CH_3I + O_2 + UV (254 nm) → CH_3O_2 + I

In the presence of excess NO, each CH_3O_2 radical produces almost two NO_2 molecules:

CH_3O_2 + NO → CH_3O + NO_2
CH_3O + O_2 → HO_2 + HCHO
CH_3O + NO + M → CH_3ONO + M
HO_2 + NO → OH + NO_2

The calibration source comprises a permeation source of CH_3I and a glass photolysis cell with a mercury UV lamp that suppresses the O_3-producing 185 nm spectral line. The CH_3I is diluted into ~10 LPM of zero air, and either passes through the UV cell or bypasses it. The difference between these two modes (through UV cell / bypass UV cell) is used to determine the CH_3O_2 mixing ratio:

$[CH_3O_2]$ = $[NO_2]$ (through UV cell) – $[NO_2]$ (bypass UV cell) / (2 * 0.92)

Where the factor of 0.92 accounts for the 8% of CH_3O radicals that form CH_3ONO rather than HO_2 at O_2 and NO mixing ratios of 20% and 1 ppm, respectively.

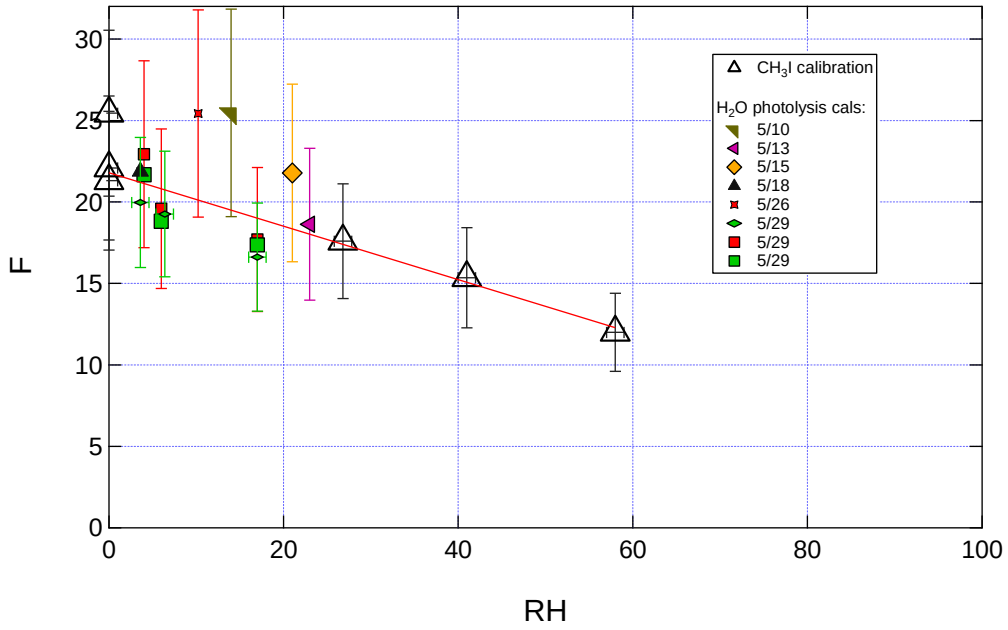

Figure 17. Amplification Factors as a function of relative humidity for the ECHAMP instrument.
The agreement between the H_2O photolysis method and the CH_3I photolysis method is within the combined uncertainties.

The results from laboratory calibrations and calibrations performed during a field deployment in Bloomington, IN during summer 2017, especially at higher RH values, will be used to finalize the instrument calibration.

Additional audits of the quality assurance includes a comparison between the Drexel NO_2 calibration method and the U. Houston NO_2 calibration source. The Drexel method is based on quantitative conversion of O_3 produced by a 2B model 305 O_3 source to NO_2 by reaction with excess NO. The U. Houston source is based on dilution of a compressed cylinder of dilute NO_2 in nitrogen (Scot Marin gases). Dilution was executed using Alicat mass flow controllers in the AML. These two calibration methods agreed within 5%, which is within their respective uncertainties (~4% for both).

Finally, all ROx data were inspected by the PI to ensure there are no periods of negative numbers beyond that expected from near-zero concentrations and the instrumental precision.

Conclusions and Recommendations for Future Work

The preliminary analysis from the data recorded during three weeks of measurements in the greater San Antonio area indicates that ozone production rates upwind and downwind of San Antonio are "moderate", with daytime values rarely exceeding 15 ppb/hr and more often between 5 and 10 ppb/hr. Although not very high compared to those observed in Houston, an O_3 formation rate of 15 ppb/hr can lead to a violation of the NAAQS if the starting (background) concentration is already elevated, e.g. 50 ppb. The highest $P(O_3)$ values were observed in air masses with elevated P(HOx) and [NO] values greater than 300 ppt. Ozone formation was almost always NOx-limited, especially during the daytime when the absolute $P(O_3)$ values were highest. This is based on two separate analyses – one based on HOx radical budgets and the other on the dependence of $P(O_3)$ on NO and P(HOx). These results suggest that reduction of NOx emissions and corresponding decreases in ambient NOx concentrations would be much more effective than VOC emission reductions at reducing ozone formation rates *in the air masses observed*. $P(O_3)$ was not observed, however, in locations in the urban core, where routine monitoring indicate NOx concentrations that at times are much higher. Due to the higher NOx concentrations, $P(O_3)$ values are possibly higher in the urban core, though it is difficult to estimate quantitatively since ozone formation may transition to being NOx-saturated. The efficacy of NOx emission reductions in reducing ozone production rates and resulting ozone concentrations may be very sensitive to the chemical regime (NOx-limited / NOx-saturated) of ozone formation in the urban core. Future work to address these questions should focus on the dependence of $P(O_3)$ on NOx, VOCs, and P(HOx) using analysis of the measurements from this project. The dependence of $P(O_3)$ on NOx inside the urban core can be investigated using monitoring data and the relations presented by this analysis, and by similar measurements in the urban core.

Any ozone reduction program would need to account for longer-term trends in emissions on a larger spatial scale. Overall NOx concentrations are decreasing in the US, and continued decreases are expected due to the continued transition from coal to natural gas and decreases in NOx emissions from diesel engines. Increases in NOx emissions Southeast (usually upwind) of San Antonio, which was suggested by satellite observations [11], may lead to increases in $P(O_3)$ and $[O_3]$ upwind of the city. Thus future work on quantifying NOx emissions and emission trends in the greater San Antonio area will greatly contribute to an improved footing on which to make recommendations for addressing ozone pollution. This includes NOx emissions from on-road traffic, electricity generation, oil and gas activities, and other sources.

References

1. Pollack, I., T. Ryerson, M. Trainer, et al., *Airborne and ground-based observations of a weekend effect in ozone, precursors, and oxidation products in the California South Coast Air Basin.* Journal of Geophysical Research: Atmospheres, 2012. **117**(D21).
2. Wood, E.C., B.L. Deming, and S. Kundu, *Ethane-Based Chemical Amplification Measurement Technique for Atmospheric Peroxy Radicals.* Environmental Science & Technology Letters, 2016. **4**(1): p. 15-19.
3. Kebabian, P.L., E.C. Wood, S.C. Herndon, and A. Freedman, *A Practical Alternative to Chemiluminescence-Based Detection of Nitrogen Dioxide: Cavity Attenuated Phase Shift Spectroscopy.* Environ Sci Technol, 2008. **42**(16): p. 6040-6045.
4. Green, T.J., C.E. Reeves, Z.L. Fleming, et al., *An improved dual channel PERCA instrument for atmospheric measurements of peroxy radicals.* Journal of Environmental Monitoring, 2006. **8**(5): p. 530.
5. Day, D.A., P.J. Wooldridge, M.B. Dillon, J.A. Thornton, and R.C. Cohen, *A thermal dissociation laser-induced fluorescence instrument for in situ detection of NO_2, peroxy nitrates, alkyl nitrates, and HNO_3.* Journal of Geophysical Research-Atmospheres, 2002. **107**(D5-D6): p. art. no.-4046.
6. Wooldridge, P.J., A.E. Perring, T.H. Bertram, et al., *Total Peroxy Nitrates in the atmosphere: the Thermal Dissociation-Laser Induced Fluorescence (TD-LIF) technique and comparisons to speciated PAN measurements.* Atmospheric Measurement Techniques, 2010. **3**(3): p. 593-607.
7. Paul, D., A. Furgeson, and H.D. Osthoff, *Measurements of total peroxy and alkyl nitrate abundances in laboratory-generated gas samples by thermal dissociation cavity ring-down spectroscopy.* Review of Scientific Instruments, 2009. **80**(11): p. 114101.
8. Atkinson, R., D.L. Baulch, R.A. Cox, et al., *Evaluated kinetic and photochemical data for atmospheric chemistry: Volume II; gas phase reactions of organic species.* Atmos. Chem. Phys., 2006. **6**(11): p. 3625-4055.
9. Mao, J., X. Ren, S. Chen, et al., *Atmospheric oxidation capacity in the summer of Houston 2006: Comparison with summer measurements in other metropolitan studies.* Atmospheric Environment, 2010. **44**(33): p. 4107-4115.
10. Mazzuca, G.M., X. Ren, C.P. Loughner, et al., *Ozone production and its sensitivity to NOx and VOCs: results from the DISCOVER-AQ field experiment, Houston 2013.* Atmos. Chem. Phys., 2016. **16**(22): p. 14463-14474.
11. Duncan, B.N., L.N. Lamsal, A.M. Thompson, et al., *A space-based, high-resolution view of notable changes in urban NOx pollution around the world (2005–2014).* Journal of Geophysical Research: Atmospheres, 2016. **121**(2): p. 976-996.
12. Schultz, M., M. Heitlinger, D. Mihelcic, and A. Volz-Thomas, *Calibration source for peroxy radicals with built-in actinometry using H_2O and O_2 photolysis at 185 nm.* J. Geophys. Res., 1995. **100**(D9): p. 18811 - 18816.
13. Faloona, I.C., D. Tan, R.L. Lesher, et al., *A laser-induced fluorescence instrument for detecting tropospheric OH and HO_2: Characteristics and calibration.* J. Atmos. Chem., 2004. **47**(2): p. 139-167.
14. Lanzendorf, E.J., T.F. Hanisco, N.M. Donahue, and P.O. Wennberg, *Comment on: "The measurement of tropospheric OH radicals by laser-induced fluorescence spectroscopy*

during the POPCORN field campaign" by Hofzumahaus et al. and "Intercomparison of tropospheric OH radical measurements by multiple folded long-path laser absorption and laser induced fluorescence" by Brauers et al. Geophys. Res. Lett, 1997. **24**(23): p. 3037-3038.

15. Liu, Y. and J. Zhang, *Atmospheric Peroxy Radical Measurements using Dual-Channel Chemical Amplification Ravity Ringdown Spectroscopy.* Analytical Chemistry, 2014. **86**(11): p. 5391-5398.